Space Sciences Laboratory
University of California
Berkeley, California 94720

A New Method of Magnetograph Observation of the Photospheric Brightness, Velocity, and Magnetic Fields

Robert Howard,
Andrew S. Tenenbaum and John M. Wilcox

Technical Report

ONR Contract Nonr 3656(26), Project NR 021 101
Partial support from NASA Grants NsG 243 and
NGR 05-003-230, and NSF Grant GA-1319.
Series No. 9, Issue No. 7

January 30, 1968

A New Method of Magnetograph Observation of the Photospheric Brightness, Velocity, and Magnetic Fields

Robert Howard

Mt. Wilson and Palomar Observatories

Carnegie Institution of Washington

California Institute of Technology

Pasadena, California 91106

and

Andrew S. Tanenbaum and John M. Wilcox

Space Sciences Laboratory

University of California

Berkeley, California 94720

Abstract

Several improvements have been made to the Mt. Wilson Observatory solar magnetograph, including changes to the guider, the Doppler compensator, and the data handling system. The improved magnetograph has been used for a new type of solar observation consisting of several hundred scans back and forth along a straight line of length 3/4 R_o perpendicular to central meridian. The data reduction, which is done entirely with a computer, eliminates those effects which have their origin in the earth-sun geometry. The spatial and temporal properties of the 5-minute oscillations are discussed.

1. Introduction

This is the first in a series of papers that will describe a new type of observation made with the Mount Wilson Observatory solar magnetograph. The emphasis on this paper will be on the equipment, the observing procedure, and the data reduction techniques, with some preliminary results given to illustrate the method. The analysis of the data is presently in progress and will not be completed for some time, since over 200 hours of data have been obtained during the summers of 1966 and 1967.

A somewhat similar observation has been made independently by DEUBNER (1967) with the Capri magnetograph of the Fraunhofer Institut. The Capri observations are recorded photographically and the Mount Wilson observations are recorded on magnetic tape, therefore details of the analysis may be quite different.

2. Instrumentation

The solar magnetograph at the 150 foot tower at Mount Wilson Observatory has evolved considerably since it was first described by H. W. BABCOCK (1953). Among the changes that will be described in this paper are a more accurate guider, an electro-optic crystal yielding an improved signal-to-noise ratio, an improved Doppler compensator, and a completely automated data recording system.

The magnetograph is fed by a vertical telescope consisting of two flat mirrors and a 30 cm, f/150 objective lens, which produces a non-rotating image 42 cm in diameter. This instrument has been described by HALE and NICHOLSON (1938). The image is guided photoelectrically by a proportional servo system. Slightly above the focal plane there is a guiding ring through which the nearly-imaged light passes (see Figure 1). Mounted 90° apart on this ring are four

pickup heads, which are designed to detect the solar limbs. They operate as two independent pairs. Only a small slice of the sun near the limb is cut out by each pickup head. The pickup heads at opposite ends of a solar diameter define an axis along which the image may be translated. Whenever the image is not centered along either axis, the corresponding pickup heads will not be equally illuminated. The light striking the guiding photocells has been deliberately diffused so that the photocells measure the total illumination in the pickup head and not the sharpness of the limb. The light from the two pickup heads on either side of a diameter is brought by means of flexible light "pipes" to one photocell. A mechanical chopper admits alternately light from one then the other head. An error signal proportional to the ac signal from the photocell drives a servo motor connected to the second flat mirror in such a way as to reduce the error signal, thereby centering the image along that axis. Under conditions of excellent seeing, the image will be kept centered in the ring to within better than one arc second. By moving the guiding ring, the solar image can be accurately moved across the entrance aperture of the spectrograph.

The guiding ring is controlled by an electronic scanning system which can translate it along either of two perpendicular axes, called x and y, as indicated in Figure 1. The basic scanning mode consists of making straight line scans in the x direction with some appropriate increment in y at the end of each scan line. The limits in x and y, the size of the y increment, the scanning speed and the starting position are all set on the control panel by the observer before the observation begins. Once the start button is depressed the scanning proceeds automatically, including a pause in the observation if a cloud passes overhead, and a continuation when the cloud has moved out of the way. Shaft encoders on the x and y drive screws continually read off the

coordinates of that part of image centered over the middle of the scanning aperture, i.e. the "position of the aperture". The aperture, of course, does not actually move, but it is simpler to refer to the "position of the aperture" rather than the "position of the image relative to the aperture". The x and y coordinates of the aperture are digitized in units of 0".284, which is about 200 km on the sun.

The right- and left-circularly polarized Zeeman components are separated by the action of an electro-optic crystal. Originally an ammonium dihydrogen phosphate (ADP) crystal was used. The ADP was replaced in early 1967 by a potassium dihydrogen phosphate (KDP) crystal, which provides a higher signal-to-noise ratio. The KDP will soon be replaced by a potassium dideuterium phosphate (KD*P) crystal, which will improve the signal-to-noise ratio still more.

The light which has passed through the "scanning" aperture is dispersed by a 22.9 meter vertical Littrow spectrograph located in a deep pit to provide very good stability. The spectrograph contains a Babcock grating 17 cm by 25 cm, ruled 600 grooves/mm, with a resolving power of over 700,000. When used with the magnetograph, the resolving power is considerably lower than this figure. The measured dispersion at the blaze angle (λ5250 in the 5th order) is 11.6 mm/A.

The magnetograph contains two completely independent exit slit assemblies, neither of which contains any slits. (One of the exit slit assemblies is not fully operational yet.) Each assembly contains two glass prisms and two moveable blinds, as shown in Figure 2. The separation between the prisms and the location of the blinds determine the "slit separation" and "slit width" respectively. The prisms and blinds (but not the lenses or photomultipliers) are mounted on an assembly which can be moved in the direction of dispersion by a

lead screw. The dc difference between the photomultiplier outputs is a measure of how far off center the spectral line is. It is used as a feedback signal to the Doppler servomotor to translate the exit slit assembly along the spectrum until the difference between the two photomultiplier outputs is zero, i.e. until the spectral line is centered between the prisms. The dynamic response of the Doppler servo is 2.2 km/sec per second of time; its natural frequency is 3 hz. Since the position of the exit slit assembly along the spectrum is a direct measure of the Doppler shift, the angle through which the lead screw has turned is also proportional to the line-of-sight velocity of the atoms forming the spectral line. A shaft encoder converts the instantaneous value of the velocity to digital form (digitized in units of about 5.2 meters/sec). The zero level of the velocity is unfortunately unknown, but it is stable over periods of at least several hours.

A simplified block diagram of the magnetograph electronics appears in Figure 3. As shown in the block diagram, three distinct signals are produced: the velocity (Doppler) signal, the magnetic (Zeeman) signal, and the intensity (brightness) signal. Before the start of each observing run, the observer selects the integration period, which may be from 0.1 seconds to 20 seconds. This determines how often a data group is recorded on the magnetic tape. At present each data group consists of six variables: the universal time to the nearest tenth of a second, the x and y coordinates of the center of the scanning aperture, the intensity, the Zeeman, and the Doppler signals. There is also room in the data group for two more channels of information. These will be chosen from among the intensity, Zeeman and Doppler signals of a second spectral line, when the second exit slit assembly and its associated electronics become fully operational. The intensity and Zeeman signals written out on the tape at the end of each integrating period are averages taken over the entire

integrating period. The Doppler signal, as well as x, y, and the universal time are the instantaneous values at the end of the integrating period. The data is written on the magnetic tape in a digital form that is compatible with the tape drives used by large digital computers, so that the entire reduction process can be done with a computer. With the usual integration period of 0.1 seconds, a typical run of three hours produces over 100,000 data groups containing over 600,000 separate pieces of information. In addition to the magnetic tape recorder, strip chart recorders and an x-y plotter are available for the observer to monitor the observing run on-line.

3. Observations

There are three general types of observations that can be made with the magnetograph. These can be approximately described as "area", "line", and "point". The first kind refers to observations covering a two dimensional area on the disk with a series of parallel scans along the x axis, each one with a slightly different value of y. These have the advantage of covering a large fraction or all of the solar disk and the disadvantage of taking a long time. For example, it would take over 5 hours to make one complete magnetogram of the entire disk with a 5" aperture. Clearly it is not possible to investigate phenomena with a time scale of a few minutes (e.g. the vertical velocity oscillations) this way. If a larger aperture is used, the observation goes faster, but the spatial resolution becomes lower, which is also undesirable. The results from an "area" observation typically take the form of three contour maps, one each for intensity, magnetic field, and velocity. Active regions are studied with such observations in order to determine the field structures correlated with chromospheric phenomena.

At the other extreme there are "point" observations, where the aperture remains almost motionless (relative to the solar image), moving only to compensate for the solar rotation. This method has the advantage of giving excellent time resolution, but little or no information about the spatial extent of the features being studied. The results of this type of observation are usually displayed as three functions of time, with autocorrelation functions and power spectra. HOWARD (1967) recently reported the results of a long series of observations of this type.

The third type of observation is the "line" observation which consists of scanning back and forth across a single straight line on the solar disk. This combines the desirable features of each of the other types: the time resolution is typically 30-60 seconds, and the distance covered can be several hundred thousand kilometers. The data presentation may be more complicated than either of the other types, and will be discussed in detail later. Most of the observations to be discussed in this series of papers will be of this type.

The x-axis was usually oriented perpendicular to central meridian. The scan line was usually within 20° of the equator, but covered a small range in latitude because B_o was never zero during the time of the observations. The length of the scan line was typically 500,000 km ($\sim 3/4$ of a solar radius). The scanning speed was generally 35.5 arc seconds per second of time, although during periods of excellent seeing it was slower by a factor of four. The scan period for the above parameters is 40 seconds, 20 seconds to go across and 20 seconds to return to the starting position. The integration time was always 0.1 seconds.

The aperture sizes varied from a circle 2".3 in diameter to a square 10" on a side, with 5" and 10" squares the most used. When the aperture was 10",

a Bowen-type image slicer was employed to avoid loss of resolution in the spectrum. In one integrating period the aperture moved a distance 3".6 along the x axis. This made the effective aperture size 10" x 13".6 for the 10" aperture and 5" x 8".6 for the 5" aperture for the intensity and magnetic signals, which are averaged over the whole integrating period. The velocity is not averaged, so for it the effective aperture size is close to the actual aperture size. Because the apertures were commonly 5" or larger, we were not restricted to conditions of especially good seeing.

The observations reported in this paper were all made with the spectral line Fe I λ 5250.216 A, chosen because it is a normal triplet with g = 3. Observations made with C I λ 5380.322, Mg I λ 5172.698, and Na I λ 5895.940 will be discussed in subsequent papers.

4. Data Reduction

Since the observations are recorded on magnetic tape, it is possible to carry out the entire reduction process using a digital computer (a CDC 6600 was used). The first step is to read the original tape, make certain corrections, and then generate a corrected tape from which all subsequent reductions will begin.

One such correction consists of changing from coordinates on the flat, stationary disk to coordinates fixed on the spherical, rotating sun. Features equally spaced on the sun will therefore appear equally spaced on the final graphs, even though these features did not appear evenly spaced on the flat image of the solar disk. Because the corrected coordinates are corotating with the sun, a solar feature that is at some coordinate x_o at the beginning of the observation will still be at x_o four hours later, even though it will have moved westward on the image by 40 arc seconds. This permits us to average

the data at any point for several hours without the solar rotation smearing it out. Although the scan line did cover a small range of latitude (usually less than 1°) the differential rotation of the sun was ignored because the variation of the rotational speed over the latitude covered by the scan line was negligible. If the scan line had been chosen parallel rather than perpendicular to central meridian, this would not have been a valid procedure.

Three main corrections are applied to the velocity signal. First, the component of the sun's rotational velocity along the line-of-sight must be removed, because it usually is much larger than the local velocity fields. A single latitude is chosen as being representative of the entire scan line, and the rotation speed for that latitude is used for all points on the scan line. The component of the rotation speed along the line-of-sight depends upon position on the sun, and is computed separately for each data group. Near the limb, where the effect is largest, it can amount to 2 km/sec. Second, the earth's rotation about its own axis contributes a component to the line-of-sight velocity. This depends primarily upon the hour angle of the sun, but also has a slight variation with position on the disk. It is a maximum at an hour angle of $\pm$ 6 hours (about 400 meters/sec), and minimum when the sun is at the zenith. The computer program generates its own ephermeris, and removes this contribution from the velocity separately for each data group taking account of the x (position) and t (universal time) coordinates for the group. The third effect is the projection of the earth's orbital velocity vector along the line of sight. This effect depends chiefly upon x, and can be as large as 150 meters/sec. As with the other geometric effects, the correction is made individually for each data group.

The net result of the above velocity corrections is to put the observer into a frame of reference located on, and corotating with, the sun. This is

consistent with the corrections made to the x coordinates. Both the velocity and position corrections are slowly varying functions of space and time. They could not possibly affect the small scale features observed in the final results.

The Zeeman signal in each data group is divided by the intensity signal in the same data group to yield the magnetic field. Since each Zeeman value is divided by an intensity measured simultaneously with it, any changes in the sky transparency will be exactly cancelled out, as will changes in the intensity due to brightness variations along the scan line. The magnetic field on the corrected tape is calibrated in gauss.

No corrections are made to the intensity signal at all. Changes in the sky transparency or in the extinction by the earth's atmosphere as the elevation of the sun changes will affect all parts of the scan line equally, providing the changes occur slowly compared to the scan period (40 seconds). Therefore results based upon comparing the intensity at one part of the scan line with the intensity at another part will still be valid even though the intensity may have been slowly changing throughout the run. This is important because the best seeing at Mount Wilson occurs shortly after dawn, when the intensity is monotonically increasing.

The eastward and westward scans are separated at this point, so that each of the final graphs will be based upon scans in one direction only. A comparison of the results based upon the eastward scans with those of the corresponding westward scans will help determine their statistical reliability.

There are several different ways that the observations can be displayed, each with certain distinct advantages. The most straightforward way to exhibit the data is to make a series of graphs of a variable (magnetic field, velocity, or brightness) as a function of position along the scan line, one graph for each scan. In order to examine quasi-permanent spatial features, it is sometimes

necessary to average the variable at each point for perhaps 30 minutes to improve the signal-to-noise ratio and to suppress such features as the well known 5-minute oscillations. Figure 4 is an example of this representation, with the graphs representing the magnetic field averaged over successive 30-minute time intervals. The dashed horizontal line is the zero field level for the first 30-minute average.

This kind of representation can be used to investigate the spatial properties of both transient and quasi-permanent phenomena, such as the sizes of certain features, spatial gradients, and relations between the velocity, intensity, and magnetic field. By subtracting each succeeding half hour average from the first one, the evolution of the various features can be emphasized.

A second representation of the data is obtained by making a series of graphs of the observations as a function of time for different positions along the scan line, rather than as a function of position for different times. A large number of evenly spaced points (typically 200) are chosen along the scan line, the spacing between adjacent points being equal to the distance traveled by the aperture in one integration period. For each of these points a graph of a variable as a function of time is prepared. An example of this representation is shown in Figure 5. The time resolution is equal to the scan period; in Figure 5 there is a point every 40 seconds. The separation between adjacent points for which the velocity is drawn is 2500 km.

5. Results and Discussion

From the graphs displaying velocity as a function of time for many different positions along the scan line, we can attempt to determine both the spatial and temporal characteristics of the 5-minute oscillations. An

inspection of Figure 5, which is typical of regions of weak magnetic fields, shows that the oscillations occupy a substantial fraction of the sun's surface at any given time. It further shows that the oscillations are irregular in amplitude and in period, and that the boundaries of coherently oscillating regions, both in space and in time, usually are poorly defined. The omnipresence of the oscillations makes an attempt to characterize them directly from graphs like Figure 5 somewhat subjective.

In order to get a more objective measure of the sizes of the oscillating regions and their coherence times, two separate procedures are employed. First, instead of plotting all the data, only those oscillations whose amplitude is greater than a certain prescribed minimum value are plotted, as in Figure 6. To separate the oscillatory from the non-oscillatory regions, it was necessary to know the zero level of the oscillatory component. For each point on the scan line, the time average of the velocity over an entire observation (4 hours 15 minutes in this case) was taken as the baseline. Only oscillations lasting at least 150 seconds are shown.

The precise results shown in Figure 6 (and graphs like it) depend somewhat upon the specific procedure used to separate the oscillatory regions from the non-oscillatory regions, particularly for oscillations shorter than one full period. The algorithm that is used is as follows: all the maxima and minima are examined (with the computer) to select out those whose amplitude is greater than some preassigned minimum value. Each point so selected identifies part of a wave train that may later be graphed. The end of the wave train is found by examining subsequent maxima and minima; the earliest one smaller than the preassigned minimum value is designated as the end of the wave train. An analogous procedure is used to identify the start of the wave train.

From a straightforward measurement, one can determine what fraction of the "area" of a graph in Figure 6 is covered by wave trains of length 10 minutes, what fraction by wave trains of length 15 minutes, etc. "Area" in this sense has dimensions of km-seconds. Figure 7 shows such a distribution for an observation which included only quiet regions. A 320-second running mean was applied to the distribution. The distribution for coherence times shorter than five minutes is not meaningful and is not shown. The area under the curve is the (average) fraction of the scan line oscillating with the specified amplitude at any given time. We find that for amplitudes of 50, 100, 150, and 200 meters/sec, 96 ± 1, 83 ± 5, 61 ± 10, and 39 ± 10 percent of the scan line is in oscillation at any instant (as observed with a 5" aperture).

A second method for investigating the spatial and temporal coherence properties consists of examining the two dimensional autocorrelation matrix A_{ij} defined by

$$A_{ij} = \frac{1}{(N-i)(M-j)} \sum_{k=0}^{N-i} \sum_{\ell=0}^{M-j} V_{k,\ell} \; V_{k+i,\ \ell+j} \qquad \begin{matrix} 0 \leq i \ll N \\ 0 \leq j \ll M \end{matrix}$$

where $V_{k\ell}$ is the velocity at the k-th point on the scan line for the ℓ-th scan, N the number of points on the scan line, and M the number of scans. Since each point on the scan line is sampled regularly every 40 seconds, the second index labels the time. The first row A_{0j} is the average of the time autocorrelation functions computed separately for each point; the row A_{1j} is the average of the cross correlation of the velocity at each point with the velocity at the adjacent point, 2500 km distant; the row A_{ij} is the average of the velocity cross correlations of all pairs of points separated by 2500i km. Figure 8 shows the first six rows of A_{ij} for a typical observation. The observation covered 500,000 km in space and 3 hours 20 minutes in time, so the

maximum lags in space and time represent 3% and 15% of the data, respectively. By connecting the maxima in the first curve of Figure 8, we arrive at an envelope from which the time required for the autocorrelation to decrease to 1/e can be found. Based upon ten hours of observations (i.e. 3 separate runs) we arrive at a characteristic decay time of 630 ± 120 seconds. The first column of the autocorrelation matrix decays to 1/e for a lag of 7700 ± km, which represents the characteristic spatial coherence length.

The numbers quoted above are averages over the entire observation. It is to be strongly emphasized that there are numerous examples of oscillations lasting much longer than 630 seconds, and extending over a distance much larger than 7700 km. For example, in Figure 5 the oscillations 148,000 km east of central meridian can be followed in time for more than 100 minutes. We also find examples of regions as large as 25,000 km in extent oscillating in phase. There are several instances in Figure 5 where a line joining maxima in the velocity at adjacent points on the sun is not quite vertical, indicating a non-zero phase velocity. A complete theory of the 5-minute oscillations will have to explain not only the mean values of the spatial and temporal extent of the oscillations, but the extreme deviations from the mean as well.

It is becoming increasingly clear that the method used to determine these mean values has a large effect on the result obtained. Using a photographic cancellation technique, LEIGHTON et al. (1962) reported an element size of 1700-3500 km (for Fe I λ6102 and Na I λ 5896 respectively). From a series of spectra, EVANS and MICHARD (1962) found a typical region of constant phase to be 2000-3000 km (for Mg I λ5173), with some regions considerably larger. DEUBNER (1967), using the Capri magnetograph, gives a typical linear distance of 4200 km (for Fe I λ5250). We do not regard our result as contradicting these earlier ones, especially since our results were based upon observations

made with a 5" aperture, which may not fully resolve the coherently oscillating regions.

It is instructive to compare the magnetic field (Figure 4) with the velocity oscillations measured simultaneously (Figure 6). The strong negative field 240,000 km east of central meridian is due to a sunspot; the area to the east of the spot is in a plage. It is obvious from Figure 6 that the 5-minute oscillations are completely suppressed in the vicinity of a spot. There is however, a hint of ordered motions in the penumbra (see Figure 9). More observations with better time resolution will be necessary to determine its nature. The plage appears to inhibit the larger amplitude oscillations more effectively than it inhibits the smaller ones.

Some of the magnetic features seen in Figure 4 evolved considerably during the course of the observation. At the beginning there were two distinct peaks in the field 435,000 km east of central meridian, each of which had a strength of about 60 gauss. The region between them gradually increased in strength, eliminating the dip between them. The reproducibility of the position of the spot and of the position and shape of the strong negative magnetic features on either side of it argue against the effect being due to a slow drift in the guiding.

Acknowledgements

The instrumental improvements in the magnetograph described here were carried out under the supervision of Dr. E. W. Dennison of the Astroelectronics Laboratory of the Mount Wilson and Palomar Observatories. This work was supported in part by the Office of Naval Research under contract Nonr 3656(26), and by the National Aeronautics and Space Administration under grants NsG 243 and NGR-05-003-230, and by the Atmospheric Sciences Section, National Science Foundation, NSF Grant GA-1319.

References

BABCOCK, H. W.: 1953, Astrophys. J. 118, 387.

DEUBNER, F. L.: 1967, Solar Physics 2, 133.

EVANS, J. W. and MICHARD, R.: 1962, Astrophys. J. 135, 812.

HALE, G. E., and NICHOLSON, S. B.: 1938, Magnetic Observations of Sunspots 1917-1924, Part 1, Carnegie Institution of Washington, Washington, D. C.

HOWARD, R.: 1967, Solar Physics 2, 3.

LEIGHTON, R. B., NOYES, R. W., and SIMON, G. W.: 1962, Astrophys. J. 135, 474.

Figure Captions

Figure 1. The solar image is kept centered in the guiding ring by the second flat servo. The guiding ring is mounted so that it can be translated in x or in y. The outer ring can be rotated and oriented so that the x motion is perpendicular to central meridian.

Figure 2. One exit slit assembly. Light from the spectrograph is incident upon the prisms, which simulate exit slits. Specially made prisms with sharp edges are used. The lenses focus the light onto the most sensitive part of the photocathodes.

Figure 3. Block diagram of the magnetograph electronics.

Figure 4. Half-hour average of the longitudinal magnetic field. The strong negative field 250,000 km east of central meridian is in a sunspot. Observations began at 1346 UT on July 17, 1966. A 10" aperture was used.

Figure 5. "Five-minute" velocity oscillations in the photosphere. The curves represent velocity as a function of time at points separated by 2500 km. Based upon same observation as Figure 4.

Figure 6. The three graphs are based on the same observation as Figures 4 and 5. The graph on the left shows only those oscillations of amplitude greater than 50 m/sec, the center graph only those oscillations of amplitude greater than 100 m/sec, and the graph on the right only those oscillations of amplitude greater than 150 m/sec.

Figure 7. Percent of the solar surface engaged in an oscillation having a certain coherence time, as a function of coherence time. The three graphs

refer to oscillations of amplitude greater than 50, 100, and 200 meters/sec. The figure is based upon 14 hours of observation made at 15°N heliographic latitude July 9-12, 1967. The aperture was 5".

Figure 8. The first six rows of the autocorrelation matrix for an observation of duration 3 hours 20 minutes made with a 5" aperture. The increase in amplitude with increasing time lag in the last two curves might possibly indicate the presence of traveling waves. HOWARD (1967) points out, however, that even an observation of 5 or 6 hours is not long enough to give reproducible autocorrelation functions.

Figure 9. Five minute oscillations in the vicinity of a sunspot, based on same observations as Figure 4. The arrows indicate the outer edges of the penumbra.

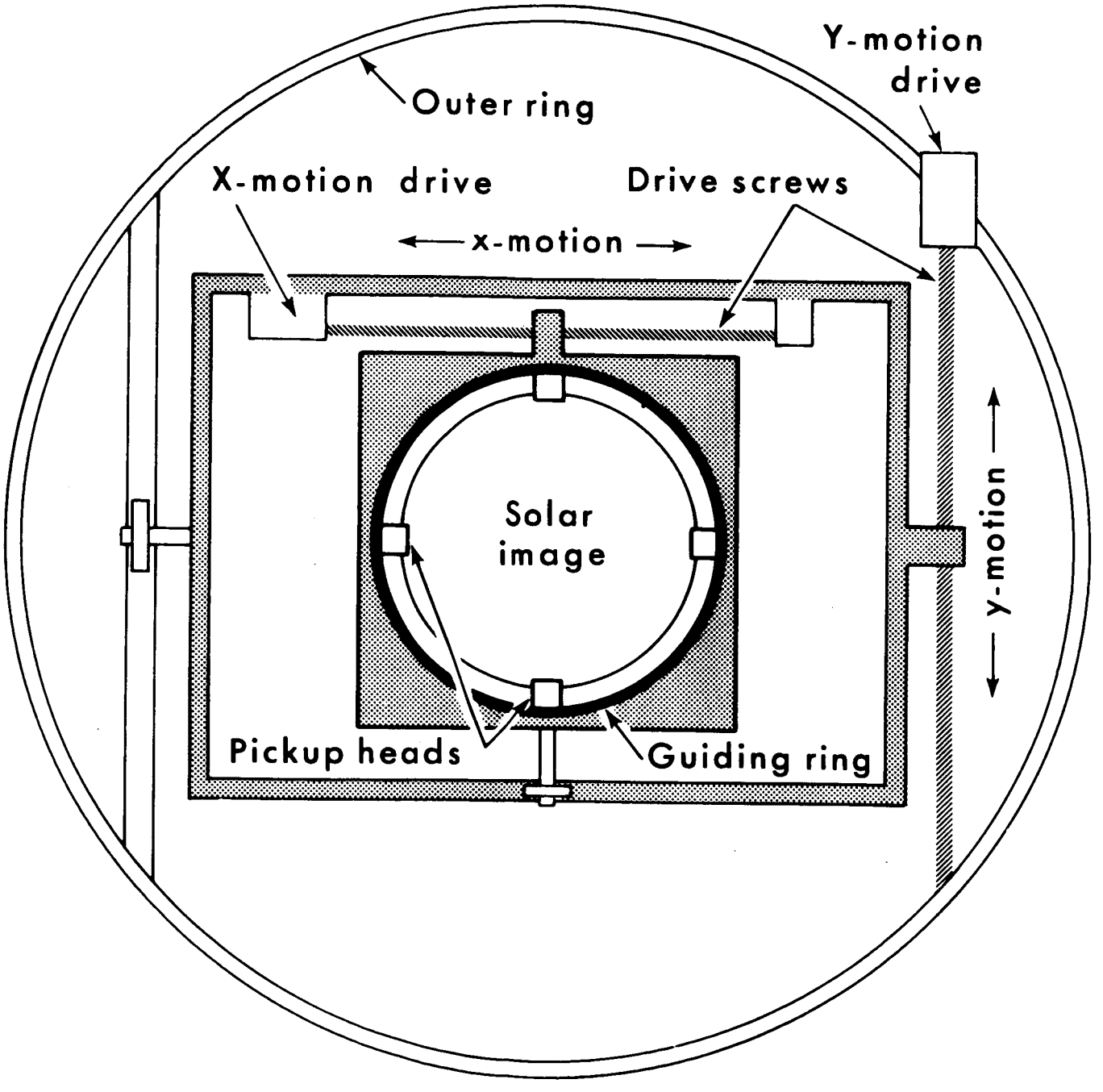
Y-motion
drive
Outer ring
X-motion drive
Drive screws
x-motion
Solar
image
y-motion
Pickup heads
Guiding ring

Figure 1

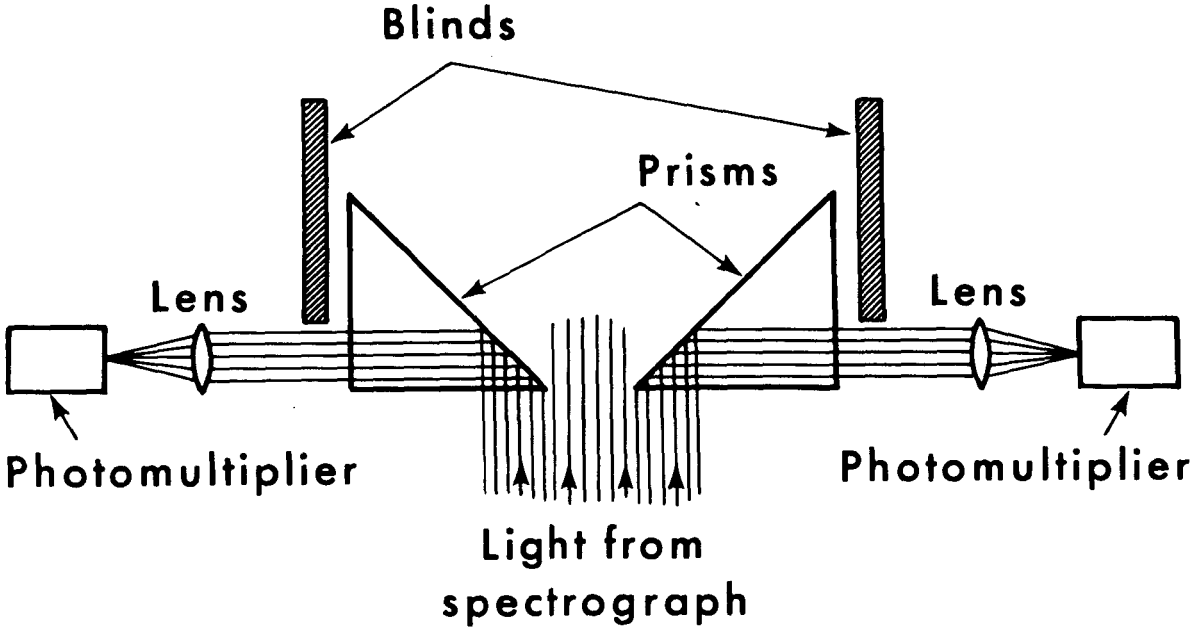
Blinds
Prisms
Lens
Lens
Photomultiplier
Photomultiplier
Light from
spectrograph

Figure 2

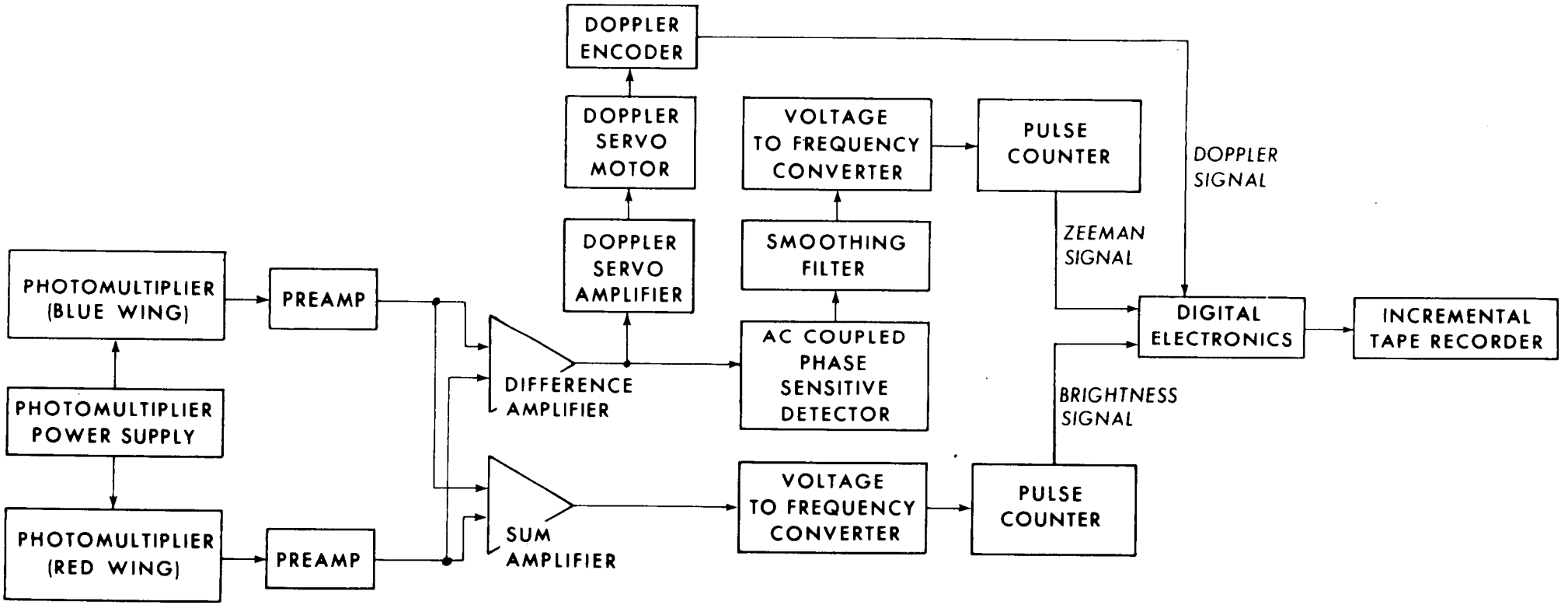
DOPPLER ENCODER
DOPPLER SERVO MOTOR
DOPPLER SERVO AMPLIFIER
VOLTAGE TO FREQUENCY CONVERTER
PULSE COUNTER
SMOOTHING FILTER
AC COUPLED PHASE SENSITIVE DETECTOR
DOPPLER SIGNAL
ZEEMAN SIGNAL
BRIGHTNESS SIGNAL
DIGITAL ELECTRONICS
INCREMENTAL TAPE RECORDER
PHOTOMULTIPLIER (BLUE WING)
PREAMP
PHOTOMULTIPLIER POWER SUPPLY
PHOTOMULTIPLIER (RED WING)
PREAMP
DIFFERENCE AMPLIFIER
SUM AMPLIFIER
VOLTAGE TO FREQUENCY CONVERTER
PULSE COUNTER

Figure 3

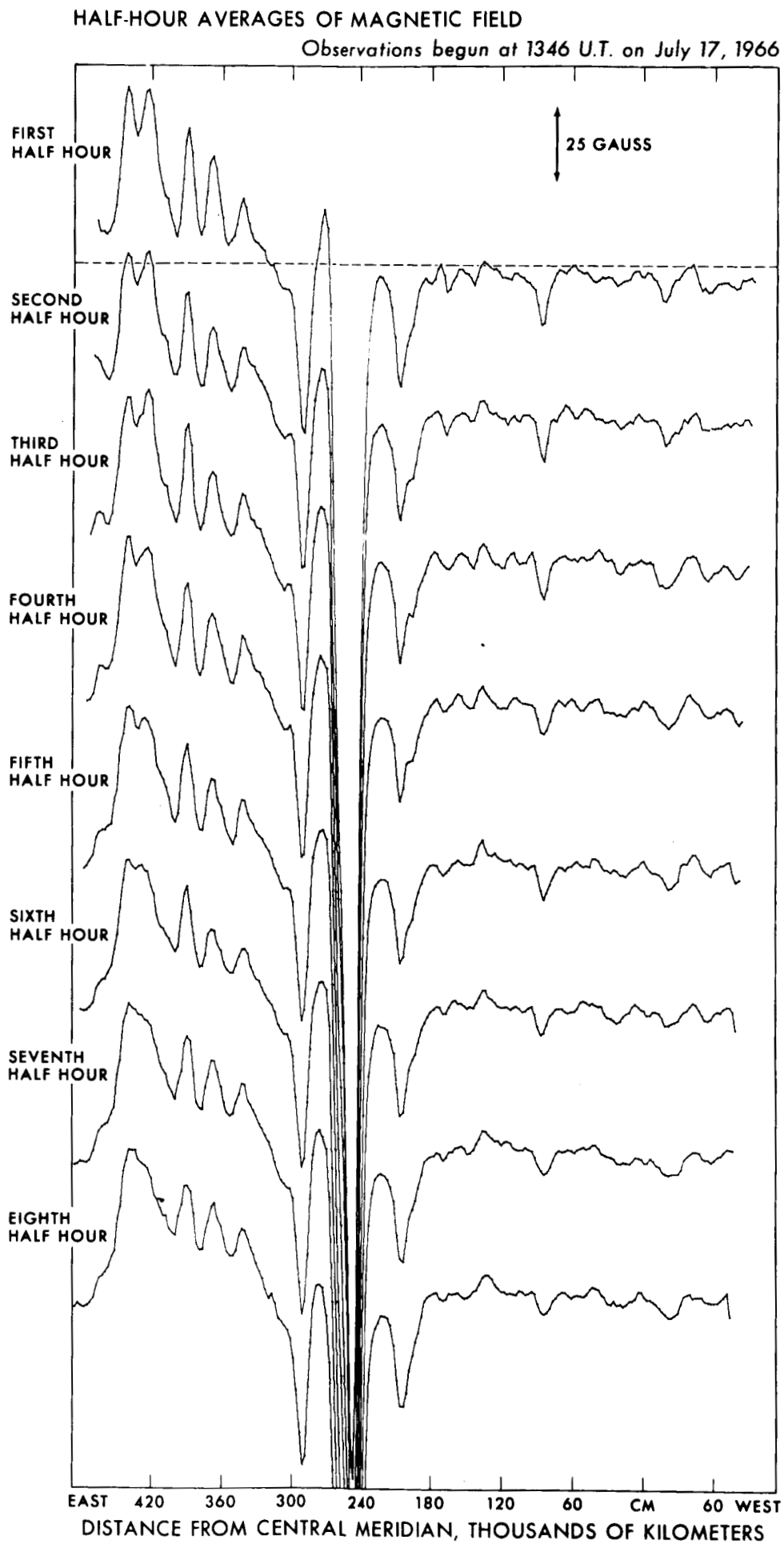
HALF-HOUR AVERAGES OF MAGNETIC FIELD
Observations begun at 1346 U.T. on July 17, 1966
25 GAUSS
FIRST HALF HOUR
SECOND HALF HOUR
THIRD HALF HOUR
FOURTH HALF HOUR
FIFTH HALF HOUR
SIXTH HALF HOUR
SEVENTH HALF HOUR
EIGHTH HALF HOUR
EAST 420 360 300 240 180 120 60 CM 60 WEST
DISTANCE FROM CENTRAL MERIDIAN, THOUSANDS OF KILOMETERS

Figure 4

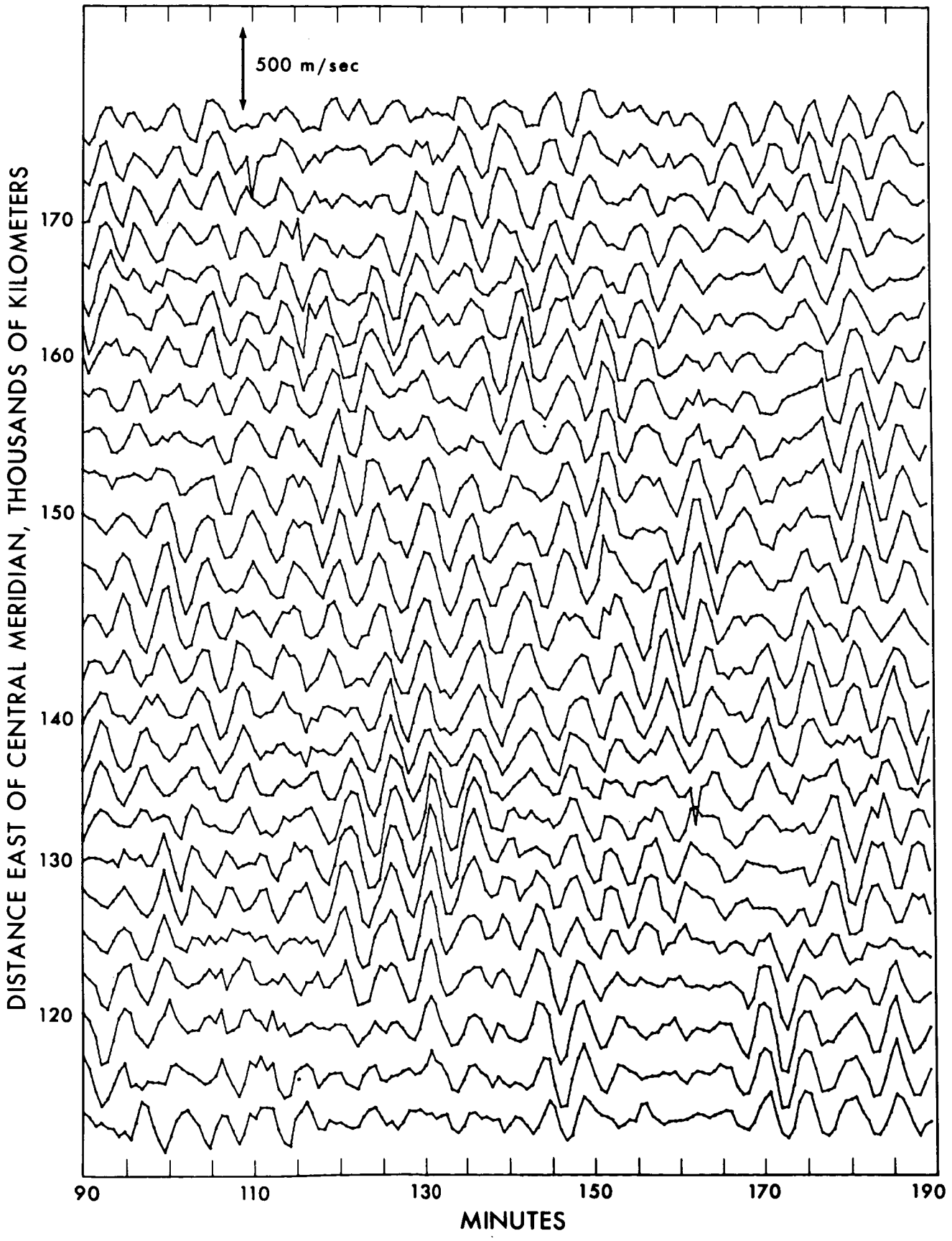
500 m/sec
DISTANCE EAST OF CENTRAL MERIDIAN, THOUSANDS OF KILOMETERS
170
160
150
140
130
120
90
110
130
150
170
190
MINUTES

Figure 5

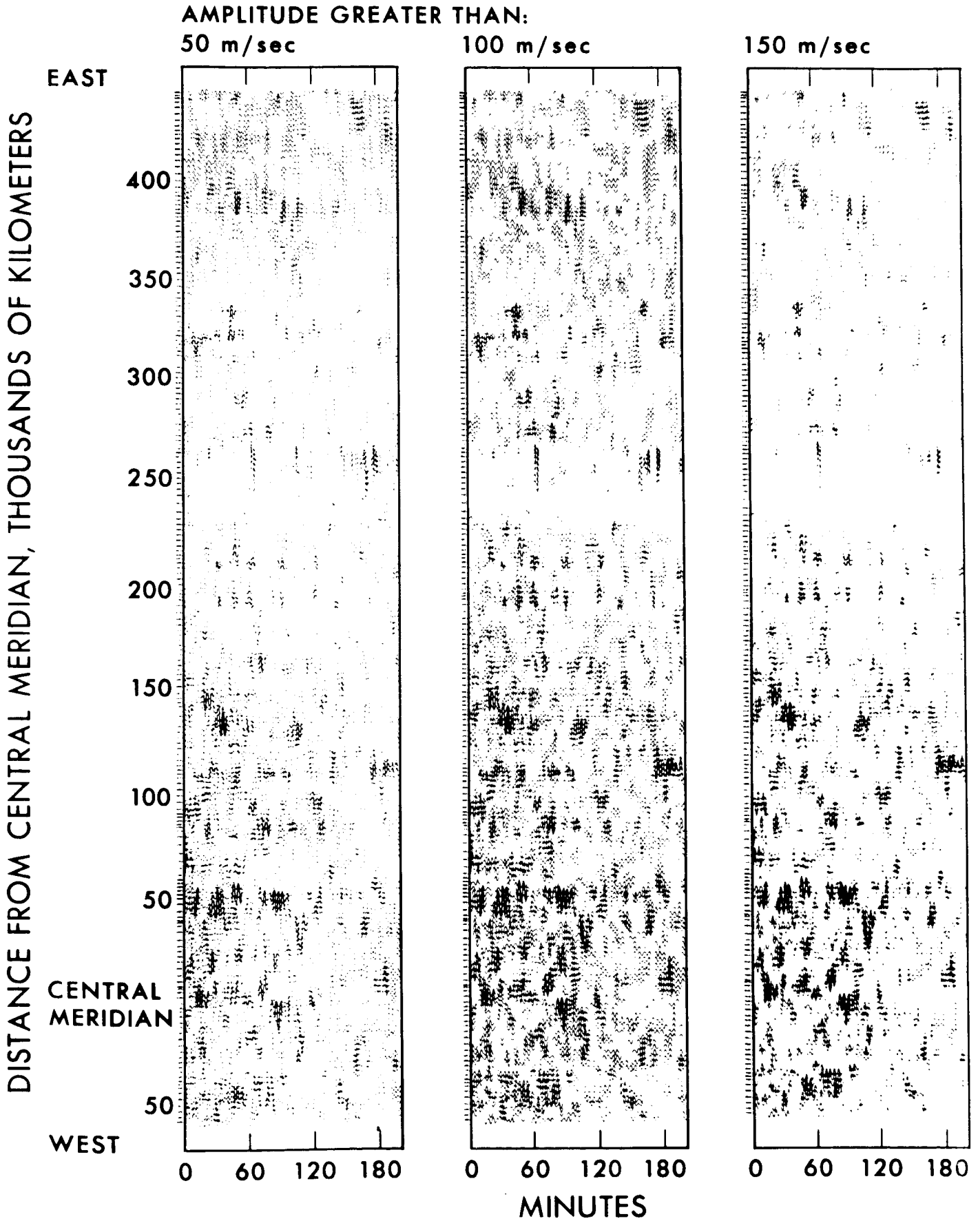
AMPLITUDE GREATER THAN:
50 m/sec
100 m/sec
150 m/sec
EAST
400
350
300
250
200
150
100
50
CENTRAL MERIDIAN
50
WEST
DISTANCE FROM CENTRAL MERIDIAN, THOUSANDS OF KILOMETERS
0
60
120
180
MINUTES

Figure 6

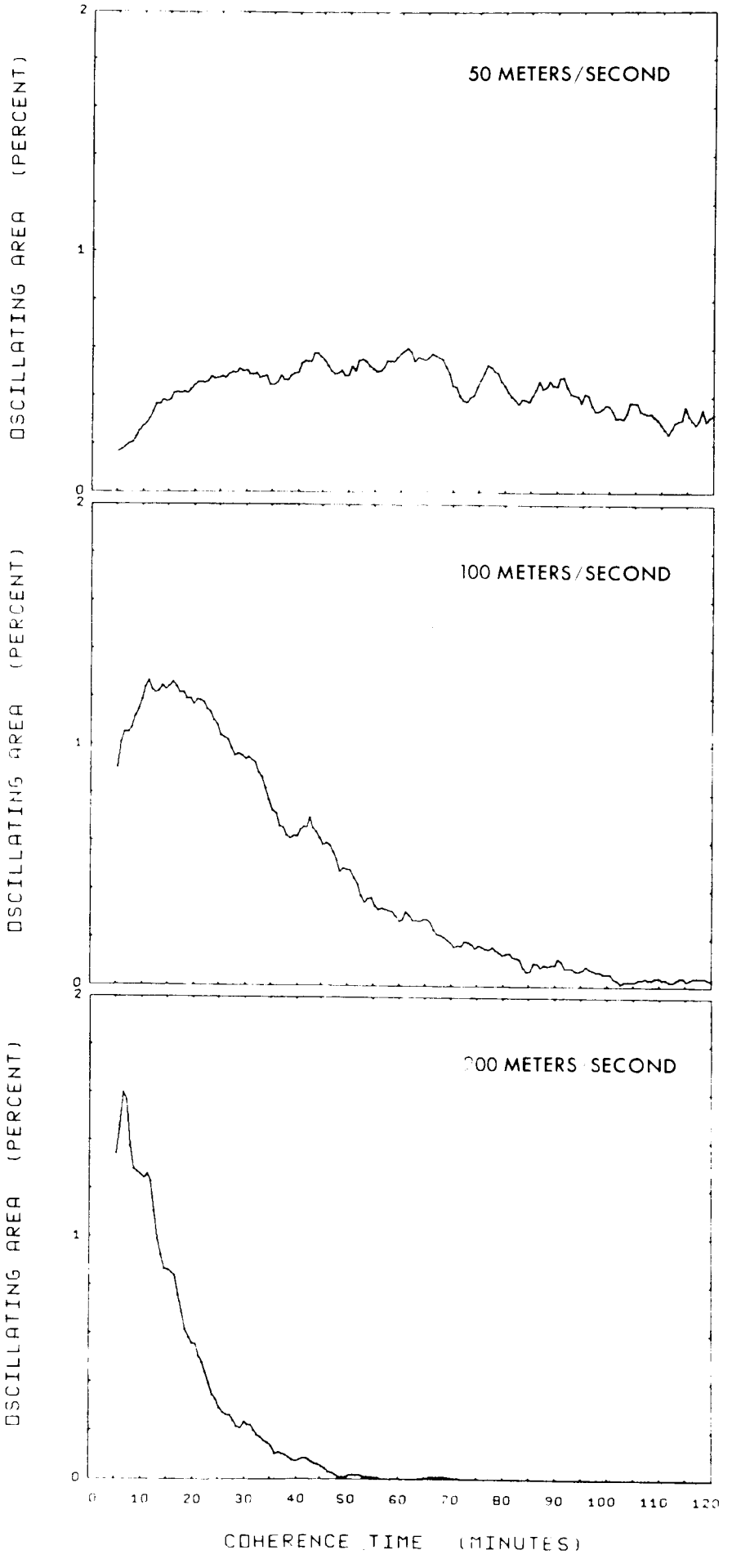
50 METERS/SECOND
100 METERS/SECOND
200 METERS/SECOND
OSCILLATING AREA (PERCENT)
OSCILLATING AREA (PERCENT)
OSCILLATING AREA (PERCENT)
2
1
0
2
1
0
2
1
0
0 10 20 30 40 50 60 70 80 90 100 110 120
COHERENCE TIME (MINUTES)

Figure

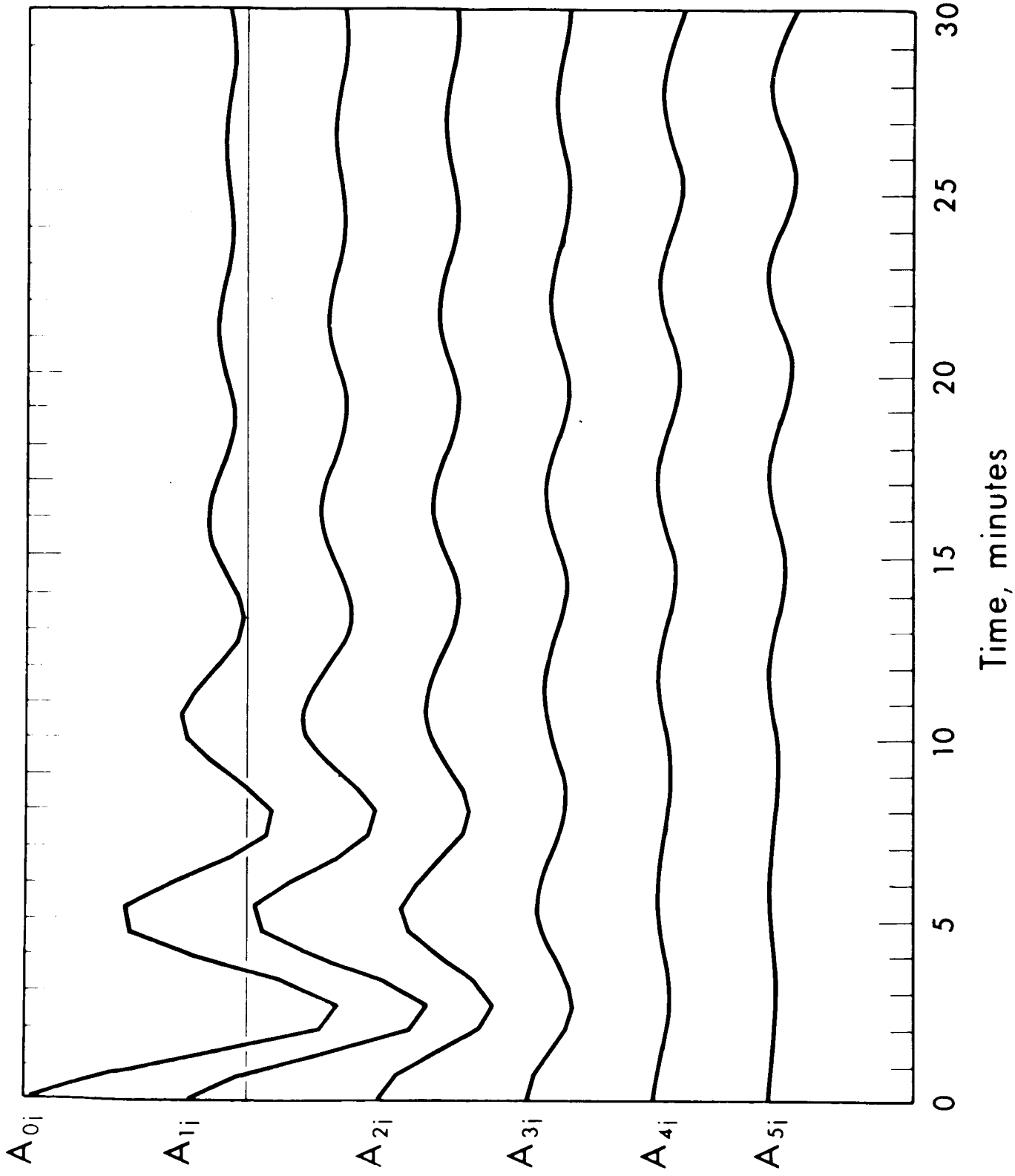

Figure 8

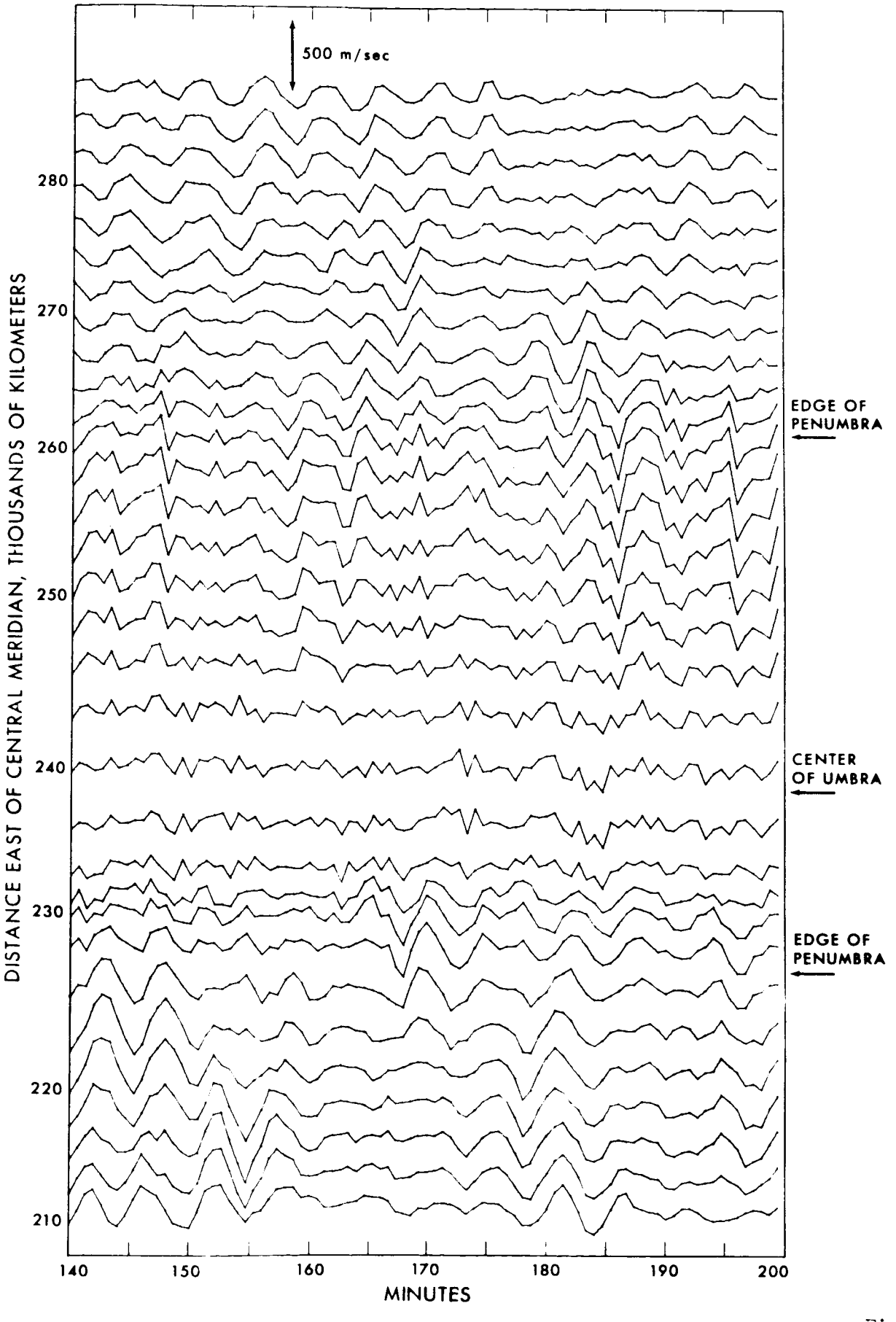
500 m/sec
280
270
260
250
240
230
220
210
DISTANCE EAST OF CENTRAL MERIDIAN, THOUSANDS OF KILOMETERS
EDGE OF PENUMBRA
CENTER OF UMBRA
EDGE OF PENUMBRA
140
150
160
170
180
190
200
MINUTES

Figure 9

UNCLASSIFIED

Security Classification

DOCUMENT CONTROL DATA - R&D

(Security classification of title, body of abstract and indexing must be entered when the overall report is classified)

1. ORIGINATING ACTIVITY (Corporate author)
Space Sciences Laboratory
University of California
Berkeley, California 94720

2a. REPORT SECURITY CLASSIFICATION
Unclassified

2b. GROUP

3. REPORT TITLE
A NEW METHOD OF MAGNETOGRAPH OBSERVATION OF THE PHOTOSPHERIC BRIGHTNESS, VELOCITY, AND MAGNETIC FIELDS

4. DESCRIPTIVE NOTES (Type of report and inclusive dates)
Technical Report

5. AUTHOR(S) (Last name, first name, initial)
Howard, Robert, Tanenbaum, Andrew S. and Wilcox, John M.

6. REPORT DATE	7a. TOTAL NO. OF PAGES	7b. NO. OF REFS
January 30, 1968	28	6

8a. CONTRACT OR GRANT NO.
ONR Contract Nonr 3656(26)
NASA Grants NsG 243 and NGR 05-003-230
NSF Grant GA-1319

b. PROJECT NO.
ONR Project No. NR 021 101

c.

d.

9a. ORIGINATOR'S REPORT NUMBER(S)
Series No. 9, Issue No. 7

9b. OTHER REPORT NO(S) (Any other numbers that may be assigned this report)

10. AVAILABILITY/LIMITATION NOTICES
Qualified requesters may obtain copies of this report from DDC

11. SUPPLEMENTARY NOTES

12. SPONSORING MILITARY ACTIVITY
Nuclear Physics Branch
Office of Naval Research
Washington, D. C. 20360

13. ABSTRACT

Several improvements have been made to the Mt. Wilson Observatory solar magnetograph, including changes to the guider, the Doppler compensator, and the data handling system. The improved magnetograph has been used for a new type of solar observation consisting of several hundred scans back and forth along a straight line of length 3/4 R_o perpendicular to central meridian. The data reduction, which is done entirely with a computer, eliminates those effects which have their origin in the earth-sun geometry. The spatial and temporal properties of the 5-minute oscillations are discussed. (U)

DD FORM 1473

UNCLASSIFIED

Security Classification

KEY WORDS	LINK A		LINK B		LINK C	
	ROLE	WT	ROLE	WT	ROLE	WT
Solar magnetic fields						
Photospheric velocity fields						
Solar magnetograph						